3 THEORETICAL FRAMEWORK

This chapter illustrates the effects of temperature changes on the Class I liquid clarification process. Basic theoretical principles are used to calculate settling velocity changes of an unhindered biofloc in water under variable temperature conditions.

3.1 Background

Theoretical MLSS settling models are required to calculate the influence of temperature on MLSS settling. The MLSS settling processes progress through 3 settling periods, as illustrated in Figure 3-1 (adapted from Ekama *et al.*, 1997). The first period (a) represents the start of the settling process at a uniform initial MLSS concentration (A). The second period (b) represents four interrelated MLSS settling processes (B, C, D, E). Liquid clarification (B), MLSS zone settling (C), MLSS transition (D), and MLSS compression (E) take place concurrently during this second period. The last period (c) represents the end of the MLSS settling processes, when the sample contains a clarified supernatant (B) and a settled MLSS (E).

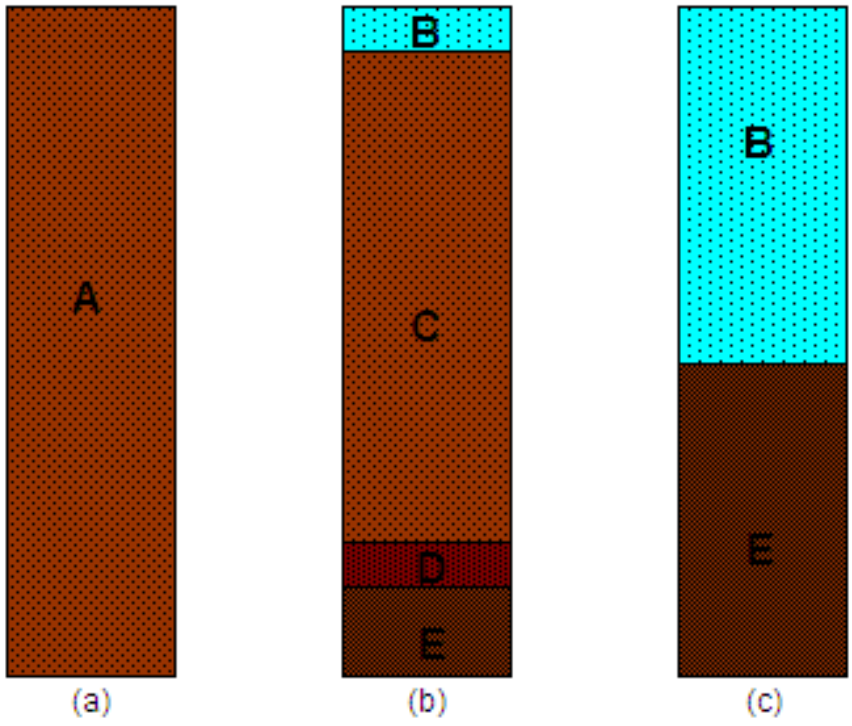

Figure 3-1 Unhindered (B) and hindered (C, D, E) settling of MLSS sample (A) in a container for three periods (a, b, c) of settling process

The hindered MLSS settling stages A and C to E are represented by simple empirical to complicated settling models based on fundamental mechanisms (Stypka, 1998). The liquid clarification stage B is represented by basic theoretical principles to describe the settling velocity of a spherical solid particle in liquid across a temperature range. In such a theoretical model, a solid particle represents a biofloc. A shape factor modifies the spherical particle to represent a non-spherical solid biofloc. This simplification excludes additional biofloc characteristics, such as porosity and biological components.

A simplified theoretical model, based on discrete, unhindered solid biofloc settling, hence represents MLSS settling. This simplified model expresses the settling velocity changes of the modified biofloc due to the effect of temperature variations on the water and biofloc characteristics.

The aim of this chapter is to illustrate the influence of temperature variations on the settling velocity of a simplified biofloc.

3.2 Materials and methods

3.2.1 Modelling approach

A simplified theoretical model illustrates the biofloc settling velocity changes over an extended operational temperature range. Variations in water viscosity and density, as well as in the key biofloc properties density, size, and shape (Scuras *et al*., 1998), are used in the biofloc settling velocity calculations.

3.2.2 Discrete biofloc settling theory

Stokes' settling model equation (Cho *et al*., 1993) calculates the unhindered settling velocity of a solid spherical biofloc in the laminar flow regime. Yuan (2001) derives Stokes' equation in detail from basic force relationships. A shape factor (Φ) is included to simulate the effect of the non-spherical biofloc shape (Gregory and Zabel, 1990) in the calculation of the biofloc settling velocity (u), valid when $Re < 1$, and $Re = 24\Phi/C_d$:

$u = (\rho_a - \rho_w)\, g\, d_a^2 / (18\mu\Phi)$,

where g is the gravitational constant, Re is the Reynolds number, and C_d is the empirical drag coefficient.

Water temperature has a direct impact on the physical state of water (Weast, 1985), in terms of the absolute water viscosity (μ) and the water density (ρ_w). Water temperature influences the physical state of the biofloc (Gerardi, 2002), in terms of the biofloc density (ρ_a), the biofloc size expressed as diameter (d_a), and Φ. The parameters representing the water and biofloc properties are varied over a range of values, as listed in Table 3-1, to determine the unhindered biofloc settling velocity changes. Average values, as indicated, are used in the simulations during the variation of each parameter.

Table 3-1 Simulation ranges used for water and biofloc characteristics

Parameter	**Average value used in simulations**	**Start of simulation**	**End of simulation**
Temperature	-	5°C	25°C
Water viscosity	-	1.523E-3 Ns/m^2	9.41E-4 Ns/m^2
Water density	998.89 kg/m^3	999.94 kg/m^3	997.08 kg/m^3
Biofloc density	1014 kg/m^3	1005.5 kg/m^3	1022.5 kg/m^3
Biofloc size	800 μm (0.8 mm)	10 μm (0.01 mm)	1410 μm (1.4 mm)
Biofloc shape	15	20	1

The water viscosity and water density variation is fixed from 1.523E-3 Ns/m^2 to 9.41E-4 Ns/m^2, and 999.94 kg/m^3 to 997.08 kg/m^3 respectively, due to the relationship with temperature over the range of 5 to 25°C (Weast, 1985). Biofloc size varies from small microflocs of 10 to 20 μm diameter (Wilén, 1999) to macroflocs up to 1400 μm diameter (Kim *et al.*, 2006), with an average diameter size range of 10 to 1000 μm (Andreadakis, 1993). Biofloc density varies from a lower range of 1015 to 1034 kg/m^3 (Andreadakis, 1993) to between 1020 and 1062 kg/m^3 (Yuan, 2001; Etterer and Wilderer, 2001). A low biofloc density range of 1005.5 to 1022.5 kg/m^3 is used to limit the rapid settling velocity increase of an single biofloc. The biofloc shape factor (Gregory and Zabel, 1990) ranges from 1 for a spherical particle up to and greater than 20 for a non-spherical biofloc.

3.2.3 Data presentation

The Microsoft Excel (Excel, 2007) curve fitting function is used to represent water density and water viscosity data in graphical format on 2-dimensional (2-D) graphs. The

coordinate system consists of the horizontal x_1-axis representing the property parameter of water as the dependent variable, and the vertical y_1-axis representing the discrete biofloc settling velocity as the response variable.

The two-input data table function of the Microsoft Excel is used to calculate the 3-dimensional (3-D) correlations. The correlations are calculated between changes in temperature (represented by water viscosity and density), the biofloc property (density, size, or shape), and the biofloc settling velocity, according to the data range in Table 3-1. The results from the calculated data are represented by the surfaces on the 3-D graphs. The bands of colour indicate changes in the settling velocity ranges, as listed in the legend box placed next to the graph. The horizontal x_1-axis and x_2-axis indicate the biofloc property and the temperature-based viscosity as the two dependent variables. The vertical y_1-axis represents the calculated discrete biofloc settling velocity as the response variable.

The coefficient of multiple determinations (R^2), as calculated by Microsoft Excel, measures the proportion of variation in the data points that are represented by the regression model. A value of R^2 equal to one means that the curve passes through every data point, while a value of R^2 equal to zero means that the regression model does not describe the data any better than a horizontal line passing through the average of the data points (DataFit, 2005).

3.3 Results and discussion

3.3.1 Temperature effect on water viscosity

The relationship between water temperature and water viscosity (Weast, 1985) is represented by an inverse polynomial equation with a R^2-value of 0.9994, as shown in Figure 3-2. The water viscosity decreases by 000058 Ns/m^2, from 1.523E-3 to 9.41E-4 Ns/m^2, as the water temperature increases from 5 to 25°C.

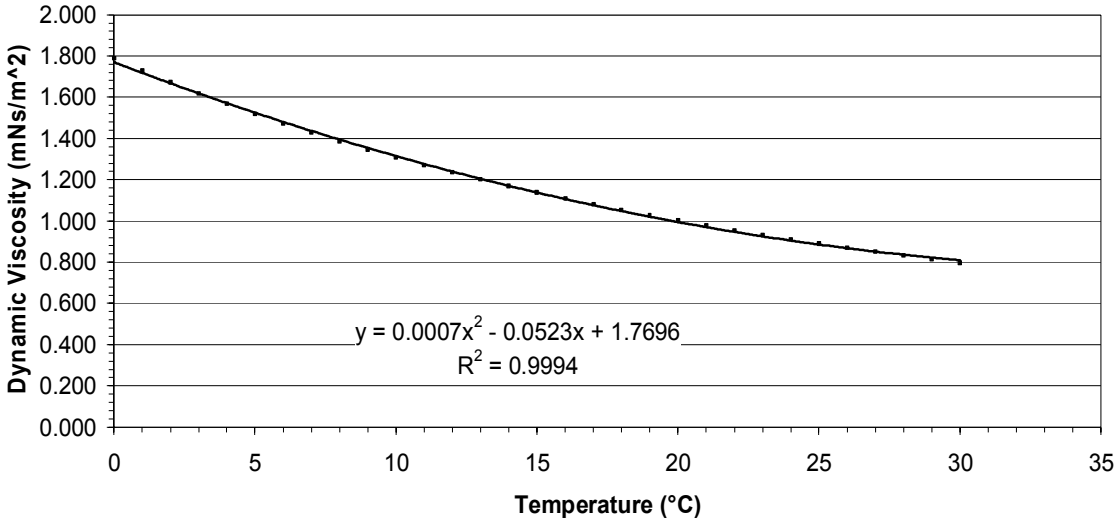

Figure 3-2 Water viscosity as a function of water temperature

3.3.2 Temperature effect on water density

The relationship between water temperature and water density (Weast, 1985) is represented by an inverse polynomial equation with a R^2-value of 0.9996, as shown in Figure 3-3. The water density decreases by 2.87 kg/m3, from 999.94 to 997.08 kg/m^3, as the water temperature increases from 5 to 25°C.

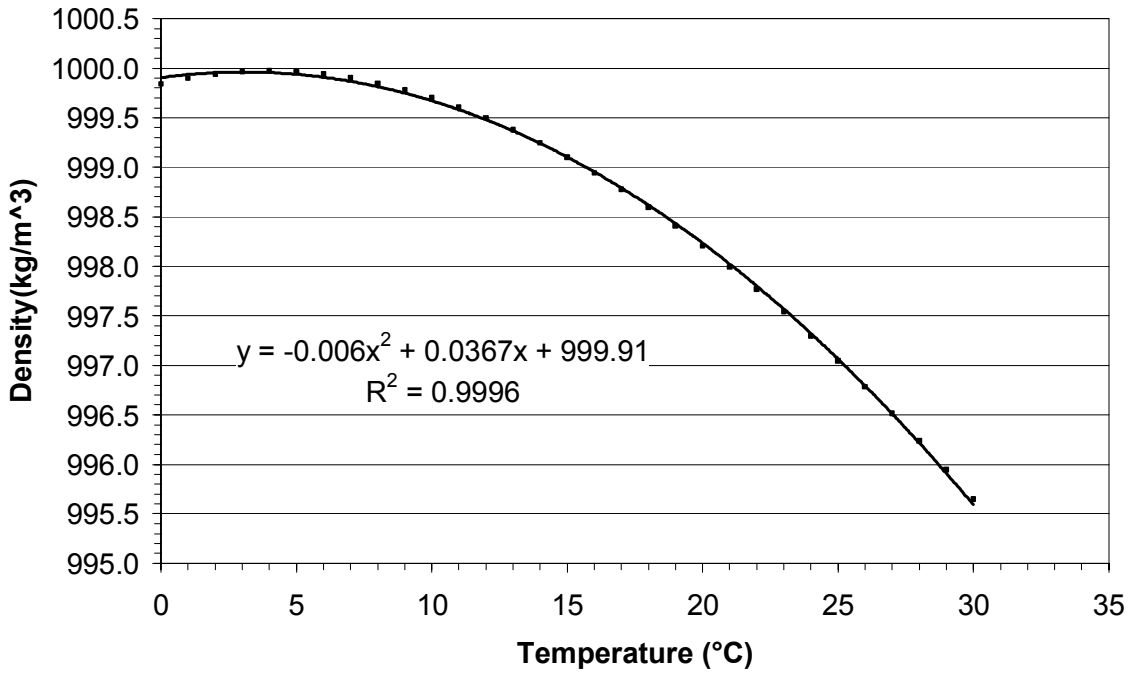

Figure 3-3 Water density as a function of water temperature

3.3.3 Settling response to water density and viscosity change

The discrete biofloc settling velocity changes due to water viscosity and water density variations over the 20°C temperature range. The change in the discrete settling velocity is graphically evaluated, to compare the different impacts of temperature related water viscosity and density variations.

The effect of a density variation on discrete biofloc settling velocity is illustrated in Figure 3-4, with a 20% velocity increase over the 20°C range. The discrete biofloc settling velocity increases by 0.14 m/hr, from 0.69 to 0.83 m/hr, due to the density decrease from 999.94 to 997.08 kg/m^3. The effect of viscosity variations on discrete biofloc settling velocity is also illustrated in Figure 3-4, with a corresponding 62% velocity increase. The discrete biofloc settling velocity increases by 0.43 m/hr, from 0.69 to 1.1 m/hr, due to the viscosity decrease from 1.523E-3 to 9.41E-4 Ns/m^2. The discrete biofloc settling velocity increases by 0.65 m/hr, from a minimum 0.69 to a maximum 1.34 m/hr, due to the combined water viscosity and density decrease of 000058 Ns/m^2 and 2.87 kg/m^3 respectively.

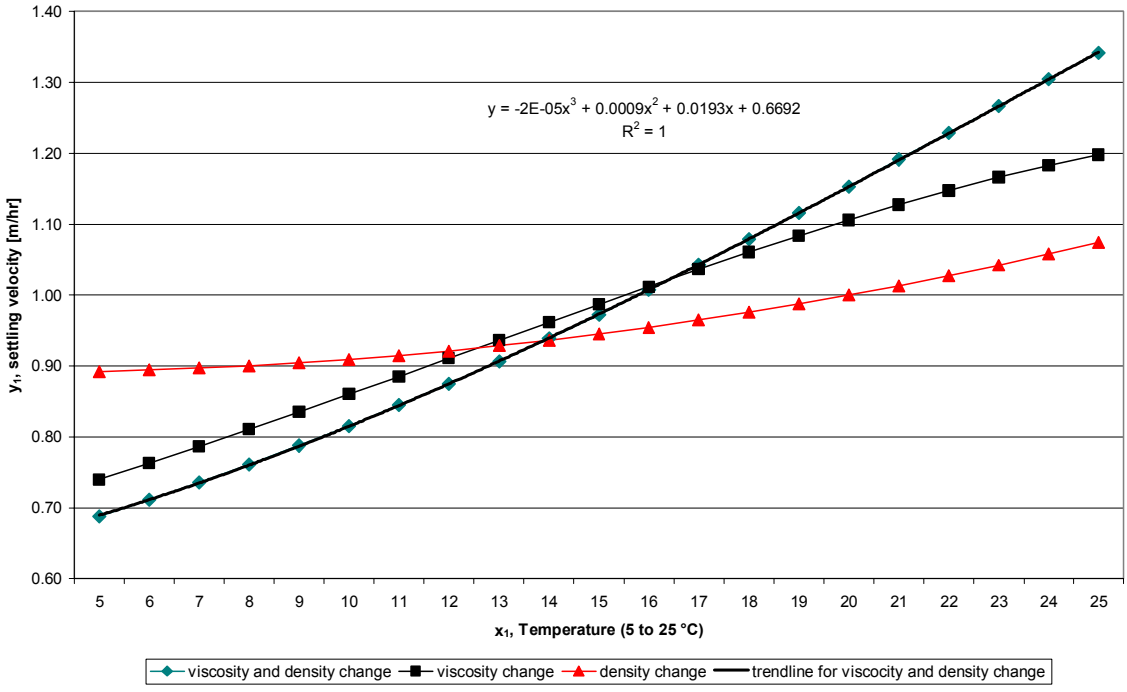

Figure 3-4 Biofloc settling velocity in water as a function of water viscosity and density

The effect of a water temperature increase over 20°C is represented by the water viscosity decrease of 0.00058 Ns/m^2 (from 0.000152 Ns/m^2 to 0.00094 Ns/m^2) and a water density decrease of 2.87 kg/m^3 (from 999.94 to 997.08 kg/m^3), to illustrate the temperature dependent settling velocity change due to biofloc density, size, and shape variations.

3.3.4 Settling response to biofloc density change

Discrete biofloc settling velocity changes, due to the combined effect of biofloc density change and temperature variation, are illustrated on the x_1-, x_2-, and y_1-axes of Figure 3-5. The settling velocity increases at the low temperature (5°C) by 15.4 m/hr, from 0.27 to 15.64 m/hr. This velocity increase originates from a biofloc density increase of 17 kg/m^3, from 1005.5 to 1022.5 kg/m^3. The settling velocity increases by 26.06 m/hr further at the higher temperature (25°C), as indicated from 0.7 to 26.76 m/hr. The velocity increase originates from the same biofloc density increase of 17 kg/m^3, from 1005.5 to 1022.5 kg/m^3.

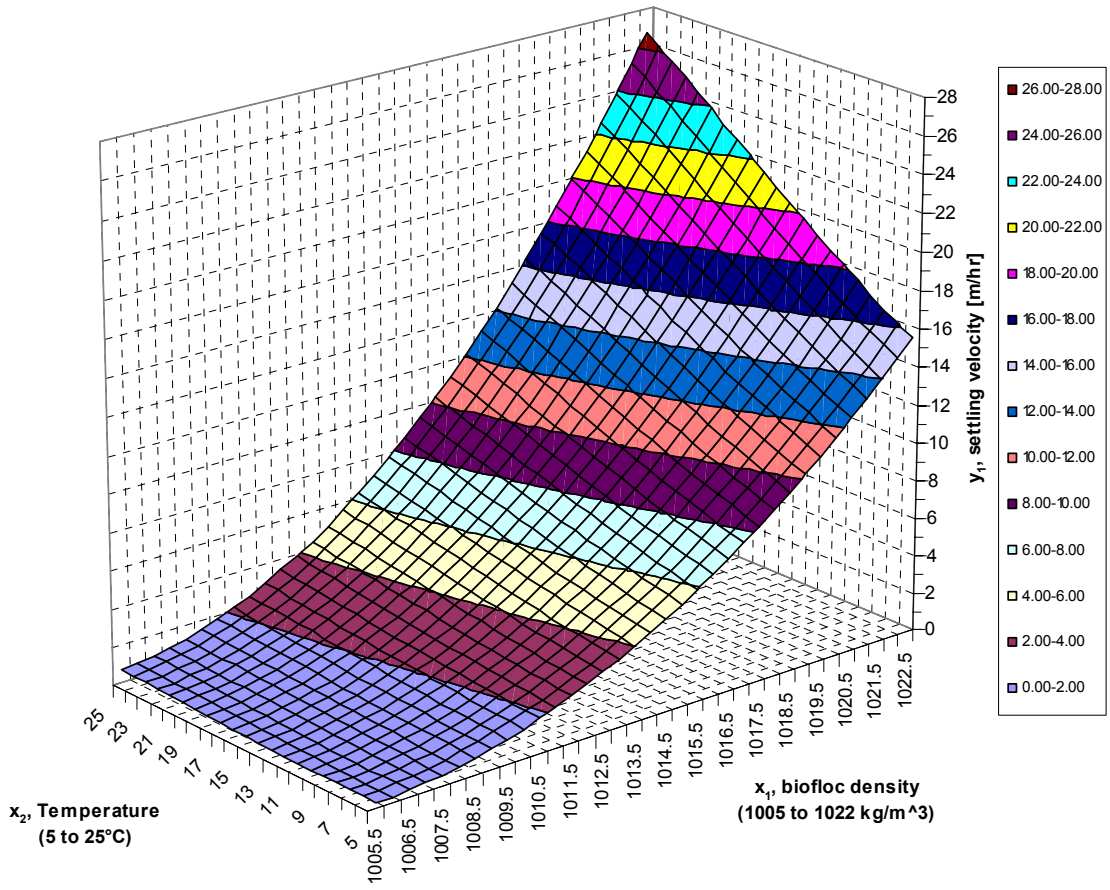

Figure 3-5 Biofloc settling velocity as a function of temperature and biofloc density

The settling velocity also increases due to a temperature increase, as illustrated on the x_2- and y_1-axes of Figure 3-5. The biofloc settling velocity increases at the low biofloc density of 1005.5 kg/m^3 by 0.43 m/hr, from 0.27 to 0.70 m/hr, due to a temperature increase of 20°C. The settling velocity increases by 11.12 m/hr further at the high biofloc density of 1022.5 kg/m^3, as indicated from 15.64 to 26.76 m/hr. The velocity increase originates from the same temperature increase of 20°C.

The discrete biofloc settling velocity increases further for a denser biofloc at a higher temperature. The settleability improves more at higher temperatures, when compared to the lower temperatures. This result is in agreement with a full-scale plant studies performed by Jang and Schuler (2006), and Schuler and Jang (2007b). These studies indicate that settleability improves with a biomass density increase, at an average SVI decrease of about 30 to 40 mℓ/g for each 0.01 g/mℓ (10 kg/m^3) density increase.

3.3.5 Settling response to biofloc size change

Discrete biofloc settling velocity changes, due to the combined effect of biofloc size change and temperature variations, are illustrated on the x_1-, x_2-, and y_1-axes in Figure 3-6. The settling velocity increases at the low temperature (5°C) by about 2.39 m/hr, from 0.0001 to 2.396 m/hr. This velocity increase originates from a biofloc size increase of about 1.4 mm, from 0.01 to 1.4 mm. The settling velocity increases by about 4.89 m/hr more at the higher temperature (25°C), as indicated from 0.0002 to 4.89 m/hr. The velocity increase originates from the same biofloc size increase of about 1.4 mm, from 0.01 to 1.41 mm.

The discrete settling velocity also increases due to a temperature increase, as illustrated on the x_2- and y_1-axes of Figure 3-6. The settling velocity increases for the small biofloc with a 0.01 mm diameter by only 0.0001 m/hr, from 0.0001 to 0.0002 m/hr, due to a temperature increase of 20°C. The discrete biofloc settling velocity increases by 2.49 m/hr further for the larger biofloc with a 1.41 mm diameter, as indicated from 2.40 to 4.89 m/hr. The velocity increase originates from the same temperature increase of 20°C.

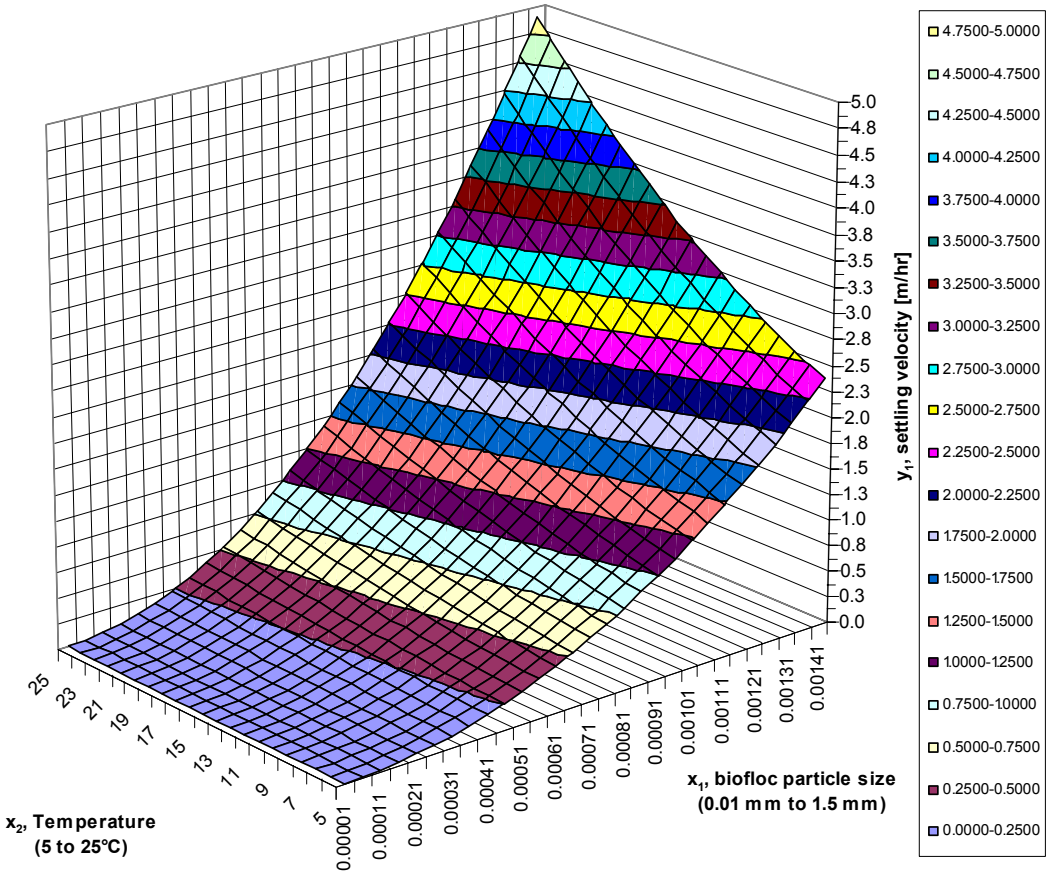

Figure 3-6 Biofloc settling velocity as a function of temperature and biofloc size

The discrete biofloc settling velocity increases therefore more for a larger biofloc at higher temperatures. The settleability improves more at higher temperatures, when compared to lower temperatures.

3.3.6 Settling response to biofloc shape change

Discrete biofloc settling velocity changes, due to the combined effect of biofloc shape change and temperature change, are illustrated on the x_1-, x_2-, and y_1-axes in Figure 3-7. The biofloc settling velocity decreases at the low temperature (5°C) by 9.78 m/hr, from 10.30 to 0.52 m/hr, due to a biofloc shape factor increase of 19, from 1 for a sphere to 20 for an irregular shaped biofloc. The biofloc settling velocity decreases by about 19.997 m/hr more at the high temperature (25°C), as indicated from 21.04 to 1.05 m/hr. The velocity decrease originates from the same biofloc shape factor increase of 19, from 1 to 20.

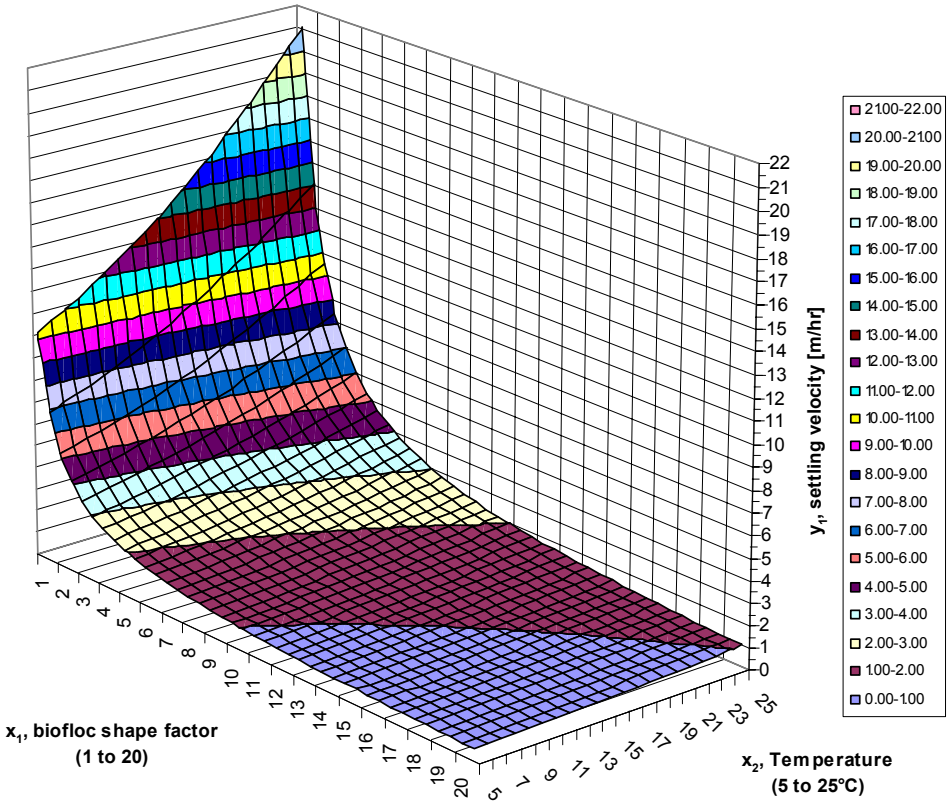

Figure 3-7 Biofloc settling velocity as a function of temperature and biofloc shape

The discrete settling velocity also increases due to a temperature increase as illustrated on the x_2- and y_1-axes of Figure 3-7. The biofloc settling velocity for the spherical biofloc increases by 10.74 m/hr, from 10.30 to 21.04 m/hr, due to a temperature increase of 20°C. The biofloc settling velocity for an irregular shaped biofloc, with a shape factor of 20, increases by only 0.53 m/hr, from 0.52 to 1.05 m/hr. The velocity decrease originates from the same temperature increase of 20°C.

The discrete biofloc settling velocity increases further for a more regular shaped biofloc, confirming results by Grijspeerdt and Verstraete (1997). The settleability improves more at higher temperatures, when compared to lower temperatures.

3.4 Summary

The Stokes model provides an indication of the unhindered settling velocity change of a simplified solid biofloc in water under influence of a temperature variation. The

temperature variation changes the effect of water (viscosity and density) and biofloc properties (density, size, and shape) on the settling velocity of the biofloc.

The predicted discrete biofloc settling velocity changes, originating from variations in water and biofloc properties, are summarised in Table 3-2. The discrete biofloc settles in all instances faster at the higher temperature of 25°C. The highest settling velocities are predicted for bioflocs with the largest density, followed by bioflocs with shape changes towards a sphere, and lastly by a larger size biofloc.

Table 3-2 Biofloc discrete settling velocity link to temperature and biofloc characteristics

Parameter	**Parameter range**	**Settling velocity at 5°C [m/hr]**	**Settling velocity at 25°C [m/hr]**
Biofloc density	1005.5 kg/m^3	0.27	0.70
	1022.5 kg/m^3	15.64	26.76
Biofloc size	1.4 mm	2.40	4.89
	0.01 mm	0.00001	0.00002
Biofloc shape	1 [-]	10.30	21.04
	20 [-]	0.52	1.05

The predicted discrete biofloc settling velocities are only valid for a solid biofloc. Additional physical changes such as porosity, and biological changes such as composition modifications, are disregarded in this evaluation. The predicted settling velocities represent only an indication of possible settling variations due to temperature fluctuations.

Hasar *et al*. (2004) identified temperature and MLSS concentration as the largest contributors to MLSS flow behaviour in a sequencing batch reactor (SBR). MLSS viscosity decreased logarithmically with a temperature increase, along with an exponential increase for a MLSS concentration increase. The basic biofloc settling calculations support these reported experimental findings, demonstrating that temperature plays a significant role in MLSS settleability.

3.5 Conclusions

The calculated unhindered settling velocity of a biofloc over a 20°C temperature range variation changes due to water viscosity and density changes, as well as biofloc density, shape, and size changes. The following conclusions are applicable for the settling biofloc:

- A water viscosity change increases the biofloc settling velocity by 0.4 m/hr, against a water density change that increases the biofloc settling velocity by 0.1 m/hr. The effect of water viscosity changes on settleability is more distinct than the effect of water density changes.

- Biofloc density is the biofloc characteristic with the largest influence on settleability in terms of settling velocity. The settling velocity increased for the denser biofloc by 11 m/hr across a 20°C increase.

- Biofloc shape is the biofloc characteristic with the second largest influence on settleability in terms of settling velocity. The settling velocity increased for the spherical biofloc by 10 m/hr across a 20°C increase.

- Biofloc size is the biofloc characteristic with the third largest influence on settleability in terms of settling velocity. The settling velocity increased for the larger biofloc by 2 m/hr across a 20°C increase.

These preliminary calculations confirm that temperature is an important dependent variable in MLSS settling. The calculations illustrate significant MLSS settling velocity changes over a temperature range variation. The next chapter will illustrate typical short- and long-term temperature variations found in a selection of operational treatment plants.

4 TEMPERATURE OBSERVATIONS

Temperature variations from an exploratory survey at five reactors are presented in this chapter. The extent of short- and long-term temperature variations illustrates typical operational temperature variation ranges. This temperature data complements the limited published information obtained from the literature survey, as well as the temperature-based settling calculations from the previous chapter.

4.1 Background

T_r is subject to short-term (hourly to diurnal) and long-term (weekly and monthly to seasonal) variations (Wahlberg *et al.*, 1996). Makinia *et al.* (2005) modelled these T_r variations as sinusoidal wave profiles that follow cyclic nighttime and winter cooling stages, between daytime and summer heating stages. The long-term T_r fluctuations are related to T_a fluctuations, which vary according to the geographical position of the plant. T_r extends from a minimum of 5 to 10°C during winter in Northern Europe and Canada to a maximum of over 30°C during summer in Asiatic countries (Oldham and Rabinowitz, 2002; Tandoi *et al.*, 2006). Long-term T_r fluctuations have a direct influence on MLSS settling. Improved MLSS settling is recorded during warmer summer months, followed by transition periods during spring and autumn (Kruit *et al.*, 2002), with poorer MLSS settling evident during colder winter months.

These long-term T_r variations govern several aspects of the biological processes, such as the rate of reactions (Krishna and Van Loosdrecht, 1999), the growth rate of all bacteria and in particular nitrifying bacteria (Barnard, 1974), as well as the selective development of specific microorganism populations (Grady and Filipe, 2000). The theoretical reaction rates for most of these biological processes double for each 10°C temperature increase up to a maximum temperature (Dochain and Vanrolleghem, 2001). Some full-scale process rates could be less temperature sensitive (Pöpel and Fischer, 1998) due to inhibiting factors.

These long-term T_r variations also influence the physical properties of MLSS. As MLSS is mainly composed of water and bioflocs (Wilén *et al.*, 2006), the physical properties relate to water characteristics such as density and viscosity, as well as biofloc

characteristics such as density, size, and shape. Short-term T_r variations influence the physical properties of MLSS, as demonstrated in the previous chapter.

Short-term T_r fluctuations are not routinely used as an operational process performance parameter. Diurnal T_r fluctuation effects on MLSS settleability are therefore not recorded or correlated to process performance. The average daily T_r of 14°C in winter and 22°C in summer for South African weather conditions are usually used as T_s for modelling exercises (WRC, 1984). The extent of MLSS T_s changes due to the influence of T_a, as well as the final difference from T_r, after a time delay due to MLSS sample collection, transfer, storage, and settling during batch tests, has not been reported in any detail in the available literature.

The aim of this chapter is to establish a typical range of plant temperature fluctuations. Differences between T_r and T_a illustrate temperature variations that can be expected between plant reactors and settling test containers under the influence of T_a.

4.2 Materials and methods

4.2.1 Experimental approach

T_r readings are recorded with hand-held or on-line thermometers at five different BNR reactors. On-line readings are continuously recorded and stored with data loggers to capture T_r profiles. These profiles are required to establish the extent of short-term temperature variations found in batch and automated MLSS settling evaluations.

4.2.2 Temperature data collection

4.2.2.1 Plant reactors used for temperature observations

Batch and on-line temperature data was collected at five BNR reactors at two wastewater plants, as indicated in Table 4-1. The size of the reactors and the aeration method are listed, as these reactor attributes could influence T_r and the extent of diurnal T_r profiles.

Plant 1 contains two full-scale reactors (1a and 1b) with surface aeration systems, as well as a pilot plant (1c) with submerged bubble aeration. Plant 2 is located about 80 km from

plant 1. Plant 2 includes adjacent surface aeration (plant 2a) and bubble aeration (plant 2b) reactors. This plant configuration offers the opportunity to identify the effects of the aeration methods on full-scale T_r.

Table 4-1 Sizes of five BNR reactors in two plants used in temperature observations

Plant	Reactor	BNR reactor size [m^3]	Aeration method
1	a	25550	Surface
1	b	15000	Surface
1	c	1.8	Bubble
2	a	45500	Surface
2	b	31796	Bubble

4.2.2.2 Short- and long-term temperature variation

On-line DO concentration meters (Royce Model 9100D; Royce, 1999) in plant 1 and 2 aerobic reactors include built-in temperature sensors. This temperature function is used to record once-off T_r readings during winter and spring at plant 1a, 2a, and 2b reactors.

These on-line DO concentration meters measure T_r continuously at plant 1b reactor. A similar DO meter was placed in the raw sewage inflow channel of plant 1 to record T_{raw}.

Data loggers (Fourier MicroLog Plus; Fourier, 2007) record the on-line data to produce diurnal T_r profiles. These data loggers contain internal temperature sensors to record T_a. Each logger produces separate T_a and T_r profiles.

4.2.2.3 Temperature data presentation

Microsoft Excel is used to plot and trend T_a, T_r, and T_{raw} profiles in graphical format in 2-D graphs. The coordinate system consists of the horizontal x_1-axis representing the time over several days or 24 hours, and the primary y_1- and secondary y_2-axes represent the temperature data.

4.3 Results and discussion

4.3.1 Long-term temperature variation

Long-term T_r variations that were recorded at wastewater treatment plants are summarised in Table 4-2. This data is based on manual readings that are listed in Table 11-1 in Appendix A. Winter T_r of surface aeration plants 1a and 2a differ by about 2°C due to geographical and local conditions. The bubble aeration plant 2b T_r is about 5°C warmer at 17 to 18°C in winter, when compared to the T_r of the adjacent surface aeration plant 2a. Spring T_r increases by about 8°C for the surface aeration reactors of plant 1a and 2a, and by 5°C for the bubble aeration reactor of plant 2b.

Table 4-2 Seasonal and daytime temperature variations: surface and bubble aeration

Plant reactor	winter morning T_r [°C]	winter afternoon T_r [°C]	spring morning T_r [°C]	spring afternoon T_r [°C]
Reactor 1a	14.2	15.0	21.6	22.0
Reactor 2a	12.1	12.7	20.6	20.5
Reactor 2b	17.7	18.0	22.8	23.0

This T_r survey confirms the extent of long-term T_r variations. The large T_r difference of more than 5°C between surface and bubble aeration at adjacent reactors of 2a and 2b has significant design and operational implications for temperature dependent BNR processes, as well as for aspects of MLSS settleability.

The T_r between morning and afternoon conditions changes by less than 1°C at all three reactors. This indicates that MLSS samples collected from the reactor during this period of the day will have a relatively constant temperature, with variations of less than 1°C in T_r. The lower afternoon T_r of 20.5°C at reactor 2a is due to a rain event. Continuous T_r profiles are preferred to identify temperature variations that might not be detected with individual readings. The T_s should also be related to T_r for batch MLSS settling tests, as different T_a can lead to changes in T_s before and during the settling tests.

The T_{raw} of plant 1 was monitored together with T_a for 42 days in spring, as shown in Figure 4-1. The T_{raw} fluctuates by 4.3°C over a range from 16.3 to 20.6°C. The cyclic T_a profile shape is similar to T_{raw} over the 42-day period, with a total change of 27°C

measured from 12 to 39°C. The placement of the small data logger enclosure in direct sunshine contributed to this extended T_a range. The T_{raw} and T_a trends follow different slopes, with T_{raw} increasing as T_a is decreasing. These trends confirm that T_{raw} is influenced by local factors other than T_a, making it difficult to predict T_{raw} profiles from T_a data.

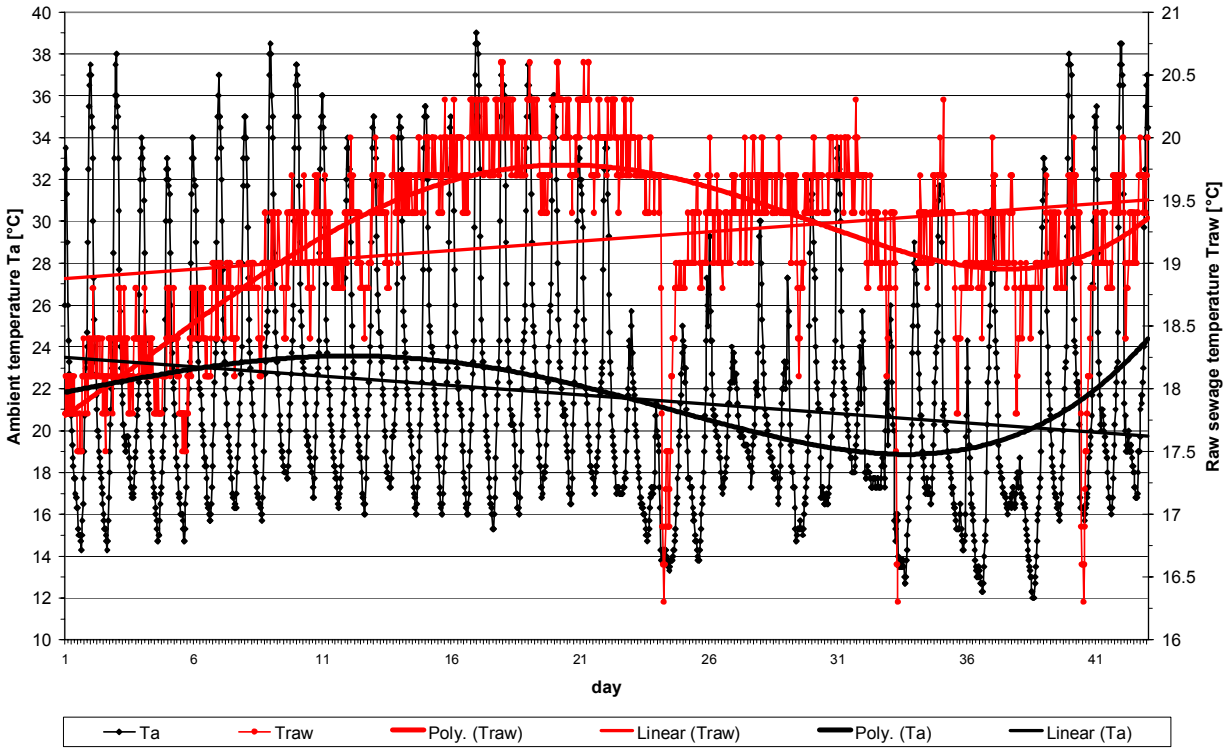

Figure 4-1 T_{raw} and T_a profiles over 42 days, plant 1

The T_r of plant 1a was monitored together with T_a for 19 days in spring, as shown in Figure 4-2. The T_r fluctuates by 2.8°C over a range from 17.2 to 20.0°C. The cyclic T_a profile shape is similar at a total change of 24.7°C, covering a range from 8.3 to 33°C. The T_r and T_a trends follow similar slopes, confirming that T_a directly influences T_r. The T_a fluctuations are mirrored by changes in the T_r. These substantial T_r changes of a few degrees Celsius occurring over several days are thus related to T_a changes.

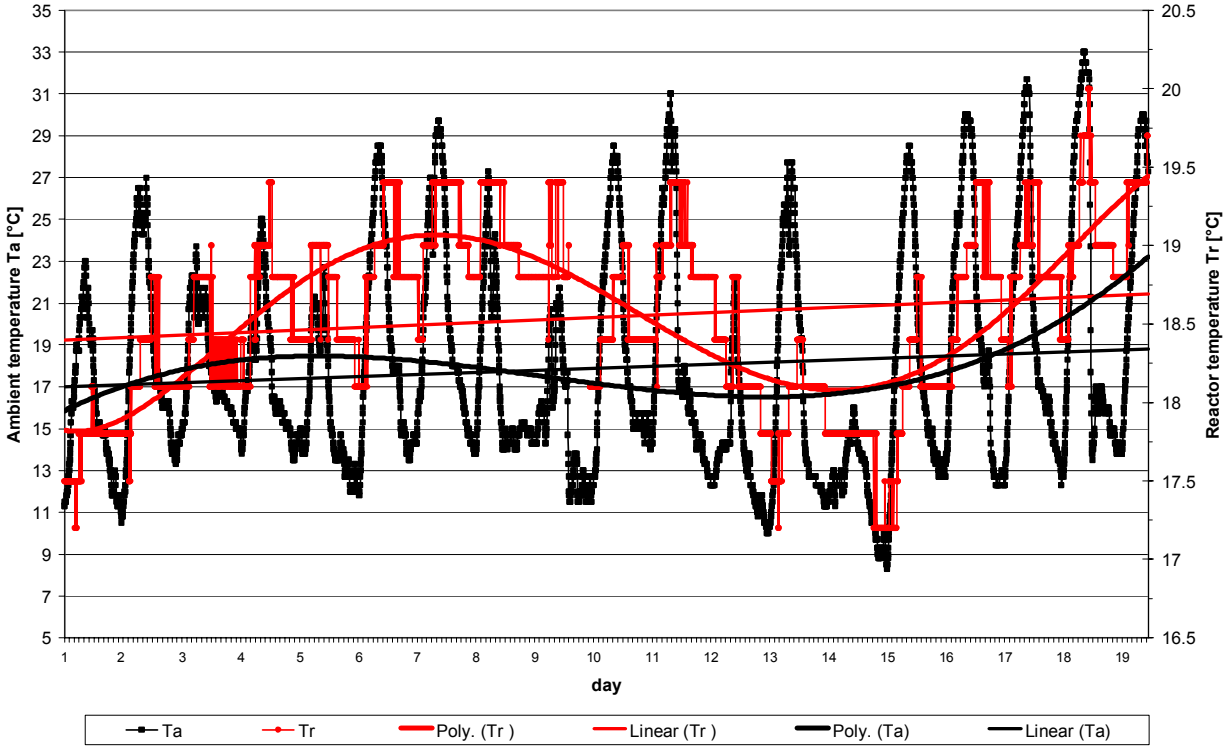

Figure 4-2 T_r and T_a profiles over 19 days, plant reactor 1a

The T_r and T_a recordings for the other two reactors at plant 1 over 10 days in spring show distinct diurnal temperature fluctuation trends. It illustrates and confirms the noticeable relationship between T_r and T_a, as shown in Figure 4-3. The T_r profile is connected by rising trend channels on the minimum and maximum daily T_r points, while the average T_r increase is shown with a linear trend line.

These trend channels indicate that the average T_r can change by approximately 4°C within 10 days at the local plants. The diurnal T_r fluctuation range increases from about 16.5 to 18°C to about 19.0 to 20.5°C, while the average linear T_r trend changes by 2.75°C, from 17.25 to 20°C. The constant slope of the trend channels illustrates that the diurnal T_r profile fluctuation stays relatively constant at about 1.5°C.

The temperature profile in Figure 4-3 also shows that the T_a increases from a diurnal variation range of about 12 to 32°C to about 16 to 30°C. The diurnal T_r variation of about 1.5°C is more constant than the diurnal T_a fluctuation that changes from about 20 to 14°C within a few days. The relationship between T_r and T_a is not constant, indicating that other factors and local conditions influence this relationship. These profiles are in good

agreement with profiles provided by Scherfig *et al.* (1996), where similar rapid temperature changes over a few days were reported.

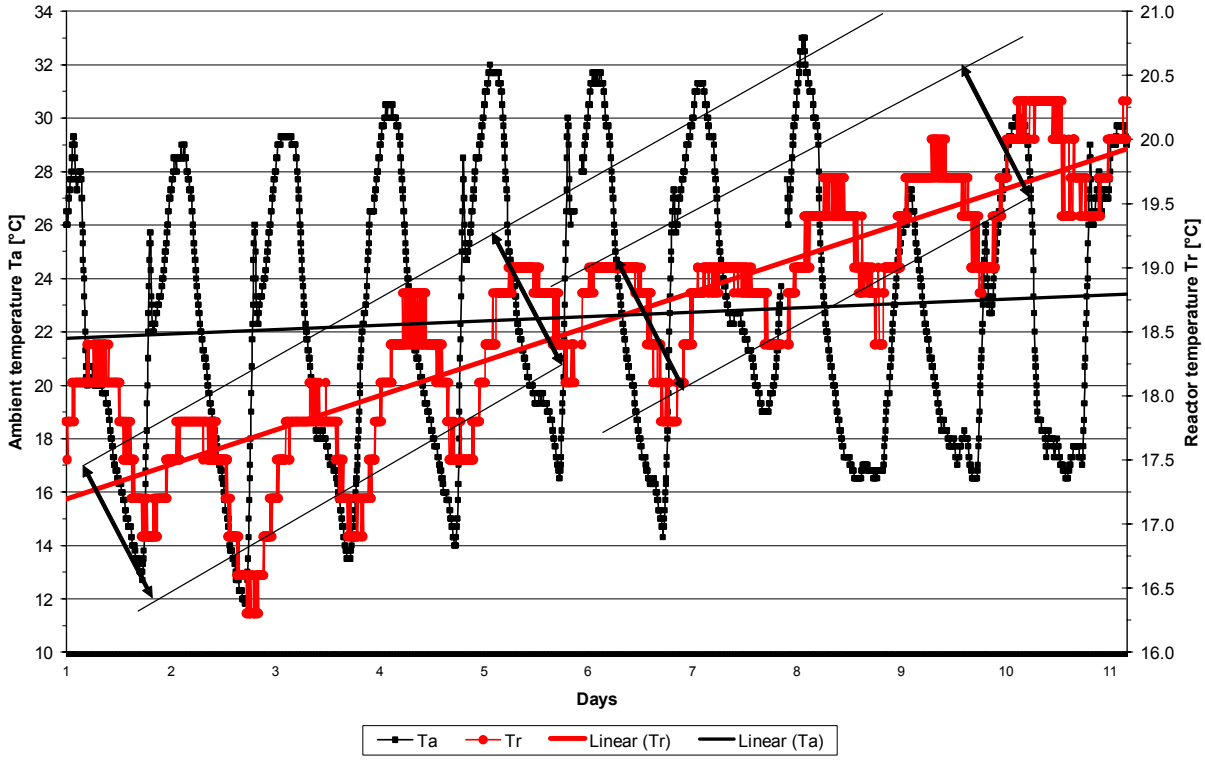

Figure 4-3 T_r and T_a profiles over 10 days, plant reactor 1b

The T_r and T_a recordings for the plant reactor 1c over an 11 day period during winter indicate more distinctive diurnal temperature fluctuation trends. It confirms the direct relationship between T_r and T_a for a smaller sized reactor, as shown in Figure 4-4. Rising trend channels on the minimum and maximum daily T_r points illustrates the T_r profile, and the average T_r increase is shown with a linear trend line.

The trend channels indicate that the average T_r can change by approximately 2°C within 10 days. The T_r diurnal fluctuation range decreases correspondingly from about 13 to 20°C to about 11 to 18 °C, corresponding directly to the changes in the T_a. The steady slope of the rising trend channels shows that the diurnal T_r profile fluctuation stays constant at about 7°C.

The profile in Figure 4-4 shows that T_a decreases from a diurnal variation range of about 4 to 20°C to about 2 to 18°C. The diurnal reactor temperature variation of about 7°C follows the T_a diurnal fluctuation of about 16°C closely, due to the small reactor size.

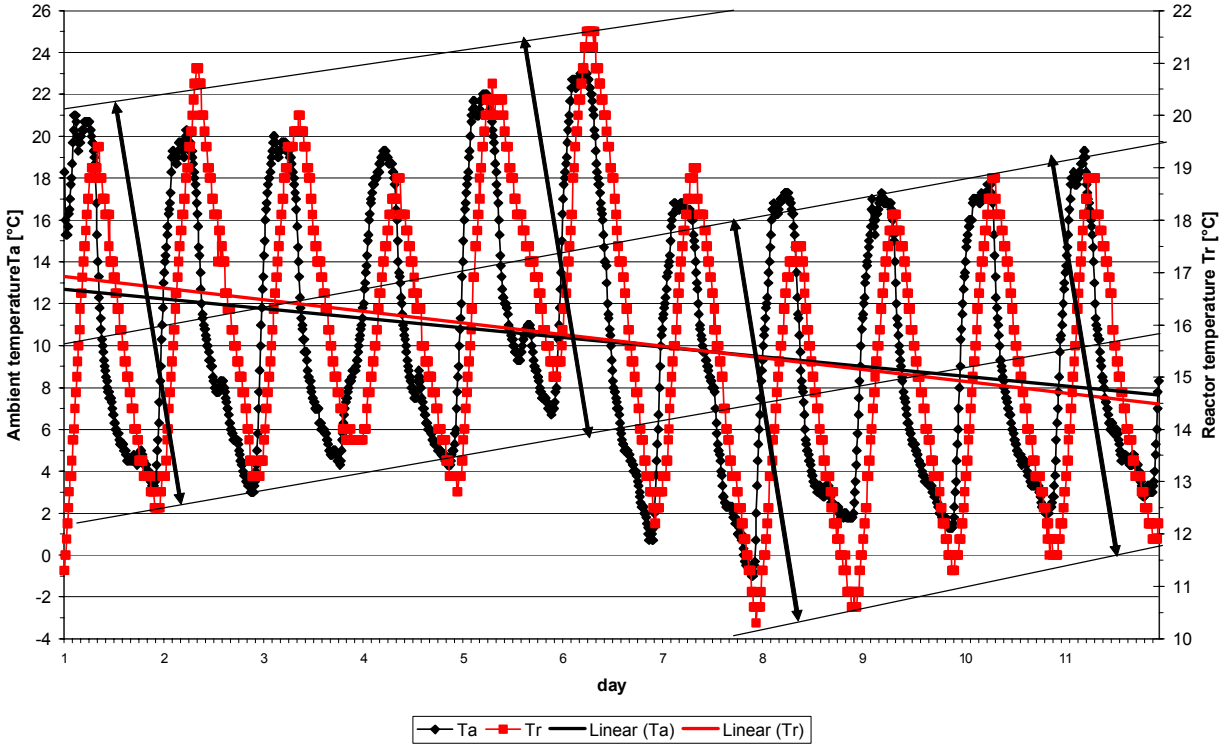

Figure 4-4 T_r and T_a profiles over 11 days, plant reactor 1c

4.3.2 Short-term temperature variations

The diurnal temperature variations for plant 1c in spring and plant reactor 1b in winter, as displayed in Figure 4-5 and Figure 4-6 respectively, illustrate the direct diurnal relationship between T_a and T_r. The T_a fluctuations are mirrored by changes in T_r, with a lag, which confirms the experimental observations of Banks *et al.* (2003).

A T_{raw} diurnal profile for plant 1 during winter, with a fluctuation of less than 1°C, is shown in Figure 11-1 in Appendix B. This profile indicates that the raw sewage temperature does not follow the diurnal T_a profile. T_{raw} cannot be represented by typical sinusoidal wave profiles, as found in cyclic T_a and T_r fluctuations.

The T_a and T_r fluctuations for a spring day are represented by polynomials with R^2 = 0.925 and 0.918 respectively. The minimum T_a of 14°C occurs at about 06:00, and the maximum T_a of 31.8 °C follows at about 15:30. The plant 1b minimum and maximum T_r are indicated from the data points as constant from about 05:00 to 10:00 at 17.5°C and 19:00 to 24:00 at 19°C respectively. These horizontal deviations from the sinusoidal wave profile are generated by the limited minimum recording limit of 0.3°C of the on-line thermometer logger. A 2-day profile is provided in Figure 11-15 in Appendix E for reference purposes, to illustrate the T_r response to T_a fluctuations. Two polynomial equations represent the T_a and T_r correlations with respective R^2 of 0.78 and 0.91.

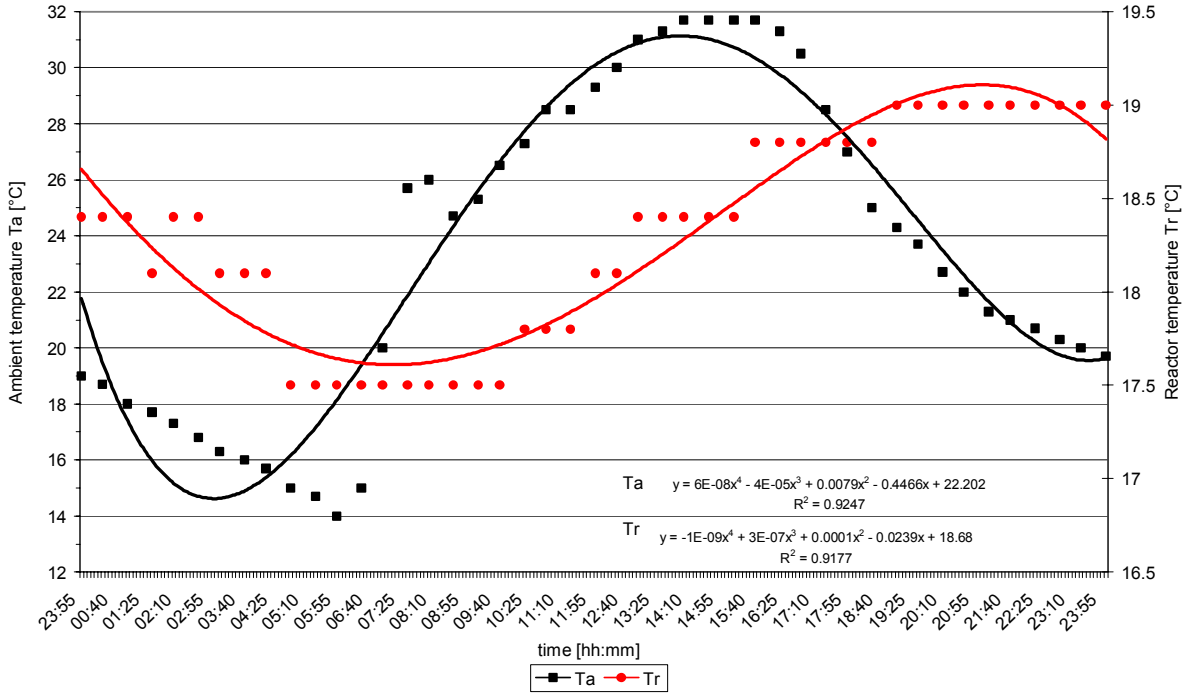

Figure 4-5 Diurnal T_r and T_a profile, plant reactor 1b

The T_a and T_r fluctuations are represented by polynomials with R^2 = 0.904 and 0.918 respectively. The plant reactor 1c T_r profile lags behind the T_a profile by only 2.5 hours. The minimum T_r of 10.9°C occurs at about 08:30, and the maximum T_r of 17.2 °C is recorded at about 21:00.

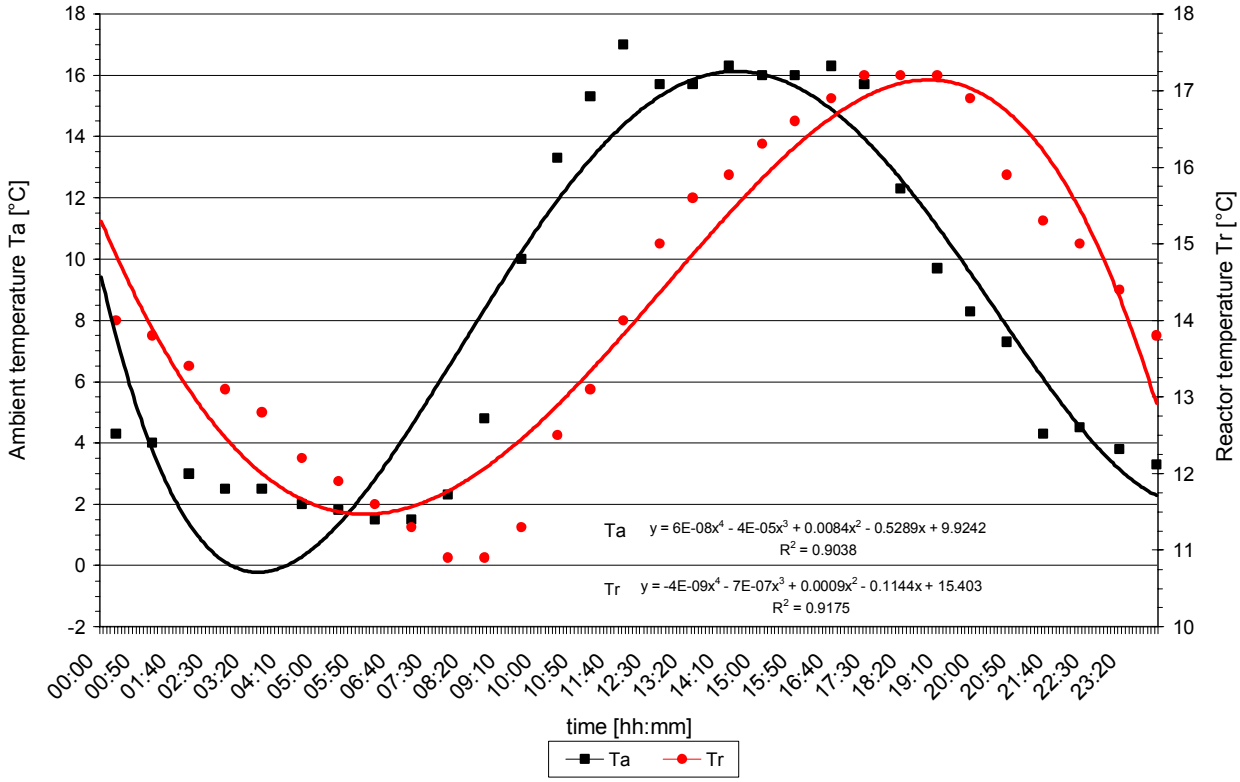

Figure 4-6 Diurnal T_r and T_a profile, plant reactor 1c

4.4 Summary

Long-term T_r variations of about 8°C are recorded from winter to spring. Reactors with surface and bubble aeration at the same plant indicated T_r differences in excess of 5°C. The increase in T_r in a full-scale plant during a week in spring has been identified at about 4°C, although the diurnal short-term T_r fluctuation of about 1.5°C stays relatively constant. This diurnal T_r variation follows a diurnal T_a variation of 14 to 32°C in spring. The winter T_a varies from 1 to 17°C, leading to an accentuated diurnal T_r fluctuation of about 7.2°C in a small pilot plant. The identified temperature variations are summarised as follows:

- Winter surface and diffused aeration systems T_r difference: 5°C,
- Winter to spring surface aeration T_r increase: 8°C,
- Winter T_a fluctuation: minimum of 1°C to maximum of 17°C,
- Spring T_a fluctuation: minimum of 14°C to maximum of 32°C,
- Monthly T_{raw} fluctuation: 4.3°C,

- Weekly T_r (full-scale) fluctuation, spring: minimum of 16.5°C to maximum of 20.5°C,
- Weekly T_r (pilot plant) fluctuation, winter: minimum of 11°C to maximum of 20°C,
- Diurnal T_r (full-scale) fluctuation in a day: 1.5°C,
- Diurnal T_r (pilot plant) fluctuation in a day: 7.2°C, and
- Diurnal T_{raw} fluctuation: <1°C.

Oldham and Rabinowitz (2002) review the application of BNR technology for cold climates in several parts of the world. The key elements in these designs are the BNR responses to low T_r conditions (presumably with surface aeration reactors). Comparable long-term low T_r conditions were identified in this temperature observation study. Reviews of BNR technology in the literature usually exclude MLSS settleability response data to these low T_r conditions.

4.5 Conclusions

The aim of this chapter is to identify operational temperature fluctuations at plant reactors. The following conclusions are based on manual temperature readings and continuous temperature profiles obtained from different reactors:

- Long-term T_{raw} changes cannot be contributed or directly related to T_a variations,
- Significant seasonal, weekly, and diurnal T_r fluctuations are recorded at plant reactors,
- Significant T_r differences were identified between surface and bubble aeration systems,
- The average T_r changes rapidly over a few days at a full-scale reactor, due to changes in T_a, as well as additional factors,
- The short-term diurnal T_r fluctuation at a full-scale reactor stays constant at 1.5°C during variations, and
- The large T_r fluctuations in a pilot plant reactor demonstrates the direct and rapid influence that meteorological conditions such as T_a has on the MLSS temperature in small containers, as found in pilot plant reactors and test cylinders.

If batch MLSS settling T_s changes significantly from these recorded T_r levels, the batch settling test results and settling parameters will be subject to variations. Batch MLSS settling test results depends on the manner in which T_r is considered during sample handling, before and during MLSS settling tests.